Available online at www.sciencedirect.com
ScienceDirect
Journal of Molecular Catalysis A: Chemical 262 (2007) 136–148
JOURNAL OF MOLECULAR CATALYSIS A: CHEMICAL
www.elsevier.com/locate/molcata

Heterogeneous photocatalysis by solid polyoxometalates

Yihang Guo [a,1], Changwen Hu [a,b,*]

[a] *Faculty of Chemistry, Northeast Normal University, Changchun 130024, PR China*
[b] *Department of Chemistry, Beijing Institute of Technology, Beijing 100081, PR China*

Available online 22 August 2006

Abstract

This paper reviews a series of novel water-tolerant polyoxometalate-containing composite photocatalysts such as amine-functionalized mesoporous silica/anatase titania impregnated with transition metal substituted polyoxometalates, bimodal porous polyoxotungstate–anatase TiO_2 nanocomposites, Fe–polytungstate–silica-structured fabrics, monovacant Keggin unit-silica/titania composite films, and highly ordered macroporous monovacant Keggin unit-titania composite films, including their design, preparation, optical absorption property, surface physico-chemical property, morphology, and heterogeneous photocatalytic behaviors. Emphases are addressed on the efficient photocatalytic activity of as-prepared solid polyoxometalates in the near UV- and/or visible-light region and easier recovery of the catalyst from the reaction system.
© 2006 Elsevier B.V. All rights reserved.

Keywords: Polyoxometalate; Heterogeneous photocatalysis; Composite films; Soft chemistry

1. Introduction

Homogeneous and heterogeneous photocatalyses have played an important role in many photochemical conversion processes, where a series of photoinduced electron transfer reactions take place on absorbing suitable energy in the near-UV or visible-light regions. Semiconductor materials including anatase TiO_2, WO_3, Ta_2O_5, ZnS, CdS, and In_2O_3 have been widely studied as the heterogeneous photocatalysts for the complete oxidation of toxic contaminants in liquid or gas phase [1–5]. On the other hand, a more complex class of photocatalytically active materials is the polyoxometalate (or heteropoly compound, abbreviated POM). POMs are well-defined early transition metal–oxygen clusters with unique structural characteristics and multiple functions, which have been significantly impacting the development of materials with catalytic, photochemical, electrochromic and magnetic properties [6]. So far thousands of POMs with different chemical composition and structure have been synthesized and characterized. In addition, the catalytic behaviors of POMs have been investigated extensively [7–11]. It shows that as the green catalysts, POMs are functioning in a variety of reaction fields, and they are also efficient multifunctional catalysts when combined with other components [12,13]. However, studies on their photooxidative behavior have received less attention compared with the semiconductor photocatalysts. In fact, many of POMs share very similar photochemical characteristics of the semiconductor photocatalysts, and POMs represent the analogues of semiconductor metal oxides [14–18]. That is, both classes of materials are constituted by d^0 transition metal and oxide ions and exhibit similar electronic attributes including well-defined HOMO–LUMO gaps (semiconductor "band gaps"). The "gaps" inhibit the recombination of electrons and holes that are generated by the irradiation of the surface of the photocatalysts with the light energy higher than or equal to their band gap energy. These photogenerated electrons and holes thus are capable of initiating the chemical reaction due to the strong photooxidative ability of the holes and photoreductive ability of the electrons. The photocatalytic reactions catalyzed by the POMs under mild reaction conditions (oxygen, atmospheric pressure, room temperature) include the oxidation of alcohol to aldehydes or ketones [19,20], the functionalization of alkanes to form alkenes or ketones [21], dimerization of alkenes [22], and degradation of all kinds of aqueous organic pollutants for advanced oxidation processes [23–25]. Most studies on the photooxidative behaviors of POMs have been with homogeneous systems, however, for the purpose of application, it is desirable to develop the photocatalytic materials in a more recoverable

* Corresponding author. Present address: Department of Chemistry, Beijing Institute of Technology, Beijing 100081, PR China. Tel.: +86 10 62828869; fax: +86 10 62828869.
E-mail addresses: guoyh@nenu.edu.cn (Y. Guo), cwhu@bit.edu.cn (C. Hu).
[1] Tel.: +86 431 5099762; fax: +86 431 5099762.

1381-1169/$ – see front matter © 2006 Elsevier B.V. All rights reserved.
doi:10.1016/j.molcata.2006.08.039

form. Therefore, water-tolerant solid POMs were prepared by combining homogeneous POMs with photoactive and inactive supporting materials (*e.g.*, silica, mesoporous molecular sieve MCM-41 or MCM-48, NaY zeolite, activated carbons, layered double hydroxide, TiO_2 in amorphous or anatase phase, and polymeric membranes) [26–32]. The specific surface areas of the supported POMs are largely increased compared with the parent POMs (BET specific surface areas of POMs are lower than $10\,m^2/g$ [9]). This larger surface area may result in an increase in the catalytic activity of POMs by providing large contact areas between the catalyst and substrate for the surface-mediated electron-transfer reactions. Another series of solid POMs are acidic Cs salts, $Cs_xH_{3-x}PW_{12}O_{40}$ ($x \leq 3$), which have porous structures, relatively high surface areas ($100–200\,m^2/g$) and strong acid sites, therefore, they exhibit excellent thermal catalytic activity and shape selectivity [12,33–36]. $Cs_3PW_{12}O_{40}$ is also the first heterogeneous POM photocatalyst used for photooxidation of propan-2-ol to acetone in an aqueous solution [37].

Most recently, many new water-tolerant POM-containing photocatalytic materials in the form of powder or membrane have been prepared. Among these composite catalysts, the inorganic precursors selected were free acids of saturated Keggin or Wells-Dawson units, paratungstate A, decatungstate, mono- and divacant Keggin units, and transition metal substituted POM (TMSP) clusters, while the selected supporters mainly were inorganic or modified inorganic porous materials so that most of the products exhibited porosities. The fascinating physical and chemical properties and unusual internal surface topology of the porous materials played important roles to improve the photocatalytic activity of POMs. In our previous review, some of these composite catalysts have been reported including silica-included microporous POMs, layered double hydroxide pillared by paratungstate A ion, surface modified mesoporous silica materials impregnated with TMSP, three-dimensionally ordered macroporous (3DOM) hybrid silica/titania materials based on monovacant Keggin-type POMs [38]. These materials were prepared by soft chemical synthesis techniques including sol–gel chemistry, intercalation chemistry, colloidal crystal templating, cluster chemistry, and hydrothermal process. And the strong chemical (*e.g.*, acid–basic, covalent or coordination bonding) but not physical interaction between the POM cluster and the support existed in the composites, ensuring little leakage of the photoactive POM from the support during the photocatalytic process [39–47]. In this review, we further demonstrate the design, preparation, optical absorption property, morphology, surface physico-chemical property and heterogeneous photocatalytic behaviors of other novel solid POMs (*e.g.*, amine-functionalized mesoporous silica/anatase titania impregnated with TMSP, bimodal porous polyoxotungstate–anatase TiO_2 nanocomposites, Fe–polytungstate–silica-structured fabrics, monovacant Keggin unit-silica/titania composite films, and 3DOM monovacant Keggin unit-titania composite films). Emphases were addressed on the efficient photocatalytic activity of as-prepared solid POMs in the UV- and visible-light region and easier recovery of the catalysts from the reaction systems.

2. Photocatalyst design and preparation

Most of water-insoluble solid POMs reported in previous works showed a very low visible-light photocatalytic activity (owing to their high band gap energy) although the enhanced UV-light photocatalytic activity compared with pure POMs was obtained. Therefore, only less than 5% of the solar light can be utilized, which is the most severe reason to restrict their technological applications on a large scale. Thus, development of the efficient POM-containing photocatalytic materials that can initiate the photooxidation reactions under visible-light irradiation is an appealing challenge. In order to design these efficient solid POM photocatalysts, following factors should be considered: (i) tuning the compositions of POMs, *e.g.*, selecting POMs with low HOMO–LUMO gap energy as the inorganic precursors; (ii) selecting suitable supports, *e.g.*, photoactive supports (TiO_2, ZrO_2, or Ta_2O_5 with proper crystal phase structure) or porous supports (*e.g.*, M41S molecular sieves), therefore, the photocatalytic activity of POMs may be enhanced due to the synergistic effect occurred during the process of photoexcitation; (iii) the chemical interaction between the POM unit and the support should exist in the composite catalysts in order to inhibit the leakage of POM from the support. According to these designing ideas, the new solid POM-containing composite photocatalysts were prepared (see below). Some of them exhibited visible-light photocatalytic activity, while the others exhibited much higher UV-light photocatalytic activity than that of the parent POMs.

2.1. Polyoxometalate-containing composite photocatalyst powder

2.1.1. Bimodal porous polyoxotungstate–anatase TiO_2 nanocomposites ($H_3PW_{12}O_{40}/TiO_2$ and $H_6PW_{18}O_{62}/TiO_2$)

Method of preparation of the $H_3PW_{12}O_{40}/TiO_2$ and $H_6PW_{18}O_{62}/TiO_2$ was sol–gel following hydrothermal treatment at a lower temperature and constant heating rate (2 °C/min). Keggin or Wells-Dawson unit, $H_3PW_{12}O_{40}$ or $H_6PW_{18}O_{62}$, was selected as the inorganic precursor, while titanium tetraisopropoxide (TTIP) was selected as the titanium source [48,49]. The sol of $H_3PW_{12}O_{40}/Ti(OTi)_x(OH)_{4-x}$ or $H_6P_2W_{18}O_{62}/Ti(OTi)_x(OH)_{4-x}$ was formed via hydrolysis of TTIP in the presence of $H_3PW_{12}O_{40}$ or $H_6P_2W_{18}O_{62}$, and then following hydrothermal treatment at 200 °C with a constant heating rate (2 °C/min). Interestingly, the products thus obtained exhibited uniform anatase but not amorphous phase structure at this low temperature (XRD results in Refs. [48,49]), which is very important for polyoxotungstate-containing composite photocatalysts. However, the products were amorphous if they were prepared by the same sol–gel method following hydrothermal treatment at 200 °C without controlling the heating rate. This result suggested that the key step obtaining the polyoxotungstate–TiO_2 composites with anatase structure at a lower temperature (200 °C) is to control a constant heating rate during the process of hydrothermal treatment. At this relatively low temperature, thermal decomposition of polyoxotungstates was avoided totally. The loading weight of the Keggin or Dawson

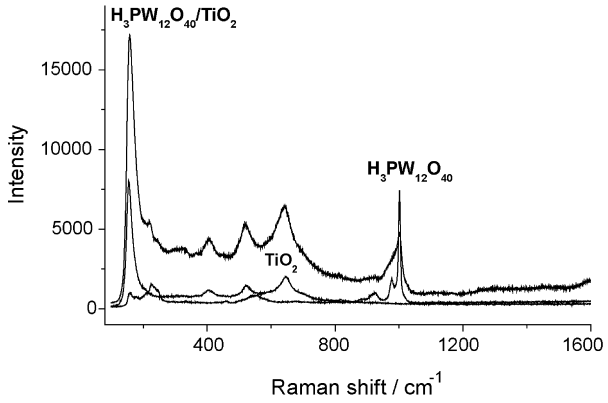

Fig. 1. Raman scattering spectra of $H_3PW_{12}O_{40}$, TiO_2, and $H_3PW_{12}O_{40}/TiO_2$.

unit in the composite could reach 19.61 or 21.52%, respectively. At this high loading weight, XRD experiment did not detect the diffraction peaks corresponding to Keggin or Dawson unit, implying their homogeneous dispersion in the anatase crystals.

Raman scattering spectroscopy rather than IR spectroscopy is an effective method to evidence the structural integrity of the polyoxotungstates after formation of the polyoxotungstate/TiO_2 composites. The reason is that the intense and broad IR vibration peaks originated from the Ti–O–Ti bonds in the TiO_2 framework severely covered the bands corresponding to P–O, W=O, or W–O–W bond vibrations from the polyoxotungstates at the mid-IR region, whereas Raman scattering signals corresponding to the polyoxotungstates can be observed in the composites. Fig. 1 shows the Raman scattering spectra of the $H_3PW_{12}O_{40}$, TiO_2, and $H_3PW_{12}O_{40}/TiO_2$. The starting $H_3PW_{12}O_{40}$-relating Raman peaks were assigned as follows: 1001.6 cm^{-1} (strong) to symmetric P–O bond stretching vibrations of the PO_4 sites; 977 cm^{-1} (weak) to W=O bond stretching vibrations, and 926 cm^{-1} (weak), to W–O–W bond stretching vibrations [49]. After impregnation of the $H_3PW_{12}O_{40}$ into anatase TiO_2 crystal lattice, the Raman peaks corresponding to the vibration of the W=O and P–O bonds were broadened, therefore, only one wide peak in the range from 935.6 to 1088.2 cm^{-1} was observed. At the same time, the peak intensity corresponding to W–O–W bond vibration became much weaker. Similar results were found in the parent $H_6P_2W_{18}O_{62}$ and $H_6P_2W_{18}O_{62}/TiO_2$ composite [49].

According to the spectroscopy data and structural characteristics of the $H_3PW_{12}O_{40}$ (or $H_6P_2W_{18}O_{62}$) and TiO_2 network, interaction between the inorganic precursor and the support, *i.e.*, hydrogen bonding and acid–basic, were inferred reasonably. That is, W=$O_t\cdots$HO–Ti, W–$O_c\cdots$HO–Ti, and W–$O_e\cdots$HO–Ti hydrogen bonds were formed between the oxygen atoms of the Keggin or Dawson anion and the surface hydroxyl groups (Ti–OH) of the anatase TiO_2, where O_t and O_c or O_e referred to the terminal oxygen atoms and the bridge oxygen atoms, respectively, in the POM units. In addition, chemically active surface Ti–OH groups were protonated in an acidic medium to form the Ti–OH_2^+ groups. The Ti–OH_2^+ group should act as a counter ion for the $H_3PW_{12}O_{40}$ or $H_6P_2W_{18}O_{62}$ unit and yielded (Ti–OH_2^+)($H_2PW_{12}O_{40}^-$) or (Ti–OH_2^+)($H_5P_2W_{18}O_{62}^-$) by acid–base reaction [48,49].

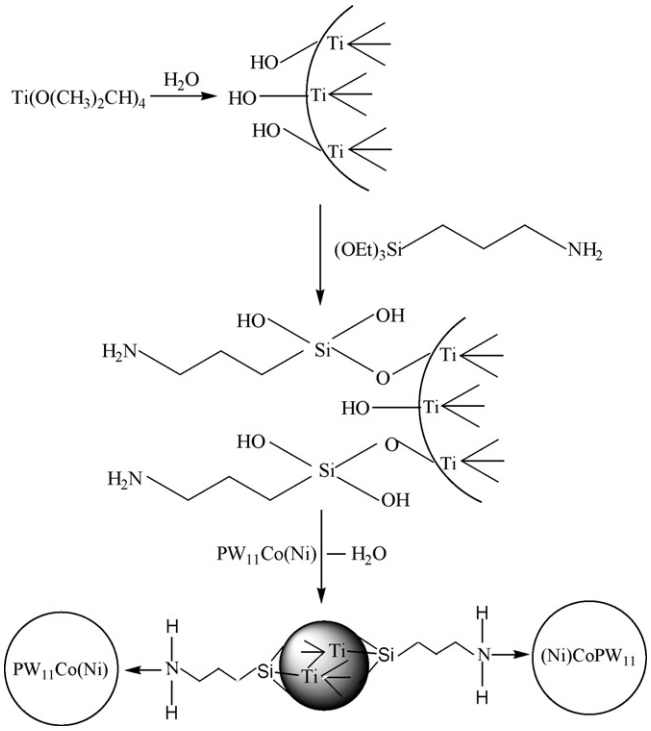

Scheme 1. Pathway of preparation of the $[Co(Ni)PW_{11}O_{39}(H_2O)]^{5-}$-APS-$TiO_2$. $[Co(Ni)(H_2O)PW_{11}O_{39}]^{5-}$ was abbreviated $PW_{11}Co(Ni)$.

2.1.2. *Amine-functionalized mesoporous silica/anatase titania impregnated with TMSP ($[M(H_2O)PW_{11}O_{39}]^{5-}$-APS-$TiO_2$, M=Co/Ni)*

For catalytic applications, the organic–inorganic hybrid solids, aminopropyl-functionalized silica materials, have been widely studied [41,49]. By using 3-aminopropyltriethoxy silane [$(EtO)_3SiCH_2CH_2CH_2NH_2$, abbreviated APS]-functionalized MCM-48 or anatase TiO_2 as the supports $[M(H_2O)PW_{11}O_{39}]^{5-}$ (M = Co/Ni) as the inorganic precursors, the hybrid photocatalysts $[M(H_2O)PW_{11}O_{39}]^{5-}$-APS-MCM-48 and $[M(H_2O)PW_{11}O_{39}]^{5-}$-APS-$TiO_2$, were prepared [51,52]. This design was based on the structure characteristic of the TMSP, that is, TMSPs are considered to be inorganic porphyrins [53,54], large inert ligands, which leave accessible coordination sites on the transition metal center. In these "inorganic porphyrins", the lacunary POM coordinates the transition metal with five O^{2-} ligands, while the last coordination site on the metal is occupied by a water molecule. The water molecule of most TMSPs can be displaced in aqueous media by ligands such as pyridines or ammonia. Therefore, TMSP was attached onto the surface of APS-silica via coordination of transition metal center in the cluster with the nitrogen atom in the surface amine groups in silica supports. Pathway of preparation of the $[M(H_2O)PW_{11}O_{39}]^{5-}$-APS-$TiO_2$ is presented in Scheme 1 [50]. Formation of the M–N coordination bond was confirmed by the FT-IR spectroscopy. That is, compared with the IR spectrum of the starting $PW_{11}Co$, a new peak (weak but sharp) appearing at 699 cm^{-1} in the IR spectrum of the $[Co(H_2O)PW_{11}O_{39}]^{5-}$-APS-MCM-48 was detected, corresponding to the vibration of Co–N coordination bond

[41,52]. In addition, the peak appearing at 3445 cm^{-1} was due to the vibration of hydroxyl groups in coordination water of the TMSP or surface hydroxyl groups of the silica support. Absorption peak appearing at 3430–3440 cm^{-1} were mainly attributed to the vibrations of N–H bonds, and the surface hydroxyl groups on the silica supporters are also responsible for this kind of vibration by formation of N–H···O–H hydrogen bonds. In these composites, propylamine groups linked to the silica surface through one or two Si–O–Si linkage, corresponding to stretching vibration in the range of 1080–1106 cm^{-1}. Absorptions ranged from 1000 to 700 cm^{-1} were due to the stretching vibrations of P–O, W–O–W, and W=O bonds of the $PW_{11}Co$ cluster. The chemical interaction (*i.e.*, M–N coordination bonding) existing between the surface of the supporter and the inorganic precursor can effectively controlled the drop of the $PW_{11}M$ cluster from the supporter (see below).

2.1.3. $H_5FeW_{12}O_{40}{\cdot}10H_2O$/silica structured fabrics

$H_5FeW_{12}O_{40}{\cdot}10H_2O$/silica structured fabrics was firstly prepared by fixing tungstoferrate(III) acid, $H_5FeW_{12}O_{40}{\cdot}10H_2O$, on a silica fabric structured matrix [55]. The silica fabric is not photoactive itself, but the photocatalytic activity of the $H_5FeW_{12}O_{40}$ was strongly enhanced by formation of the $H_5FeW_{12}O_{40}{\cdot}10H_2O$/silica structured fabrics. The deposition of the $H_5FeW_{12}O_{40}$ on the silica fabric was obtained via hydrolysis of tetraethylorthosilicate (TEOS) in the presence of $H_5FeW_{12}O_{40}$, and then the product was formed by immersing the silica fabric in the $H_5FeW_{12}O_{40}$/silica sol three times.

2.2. Polyoxometalate-containing composite photocatalyst films

Preparation of POM-containing films is a new way of immobilization of soluble POMs [56,57]. From the standpoint of practical application, formation of the POM-containing composite film is a very effective method to recover the catalyst from the reaction systems. Techniques of preparation of the composite films mainly included (i) layer-by-layer (LBL) self-assembly [58,59]; (ii) Langmuir–Blodgett (LB) deposition [60]; (iii) electrochemistry [61]; (iv) sol–gel technique [61]; (v) sputtering [62]; (vi) vacuum evaporation [63]. Among all the techniques mentioned above, sol–gel method via spin coating has obvious feasibility and easy control properties. In this way, monovacant POM–silica/titania composite films were prepared by selecting TEOS or $Ti(OC_4H_9)_4$ as the silicon or titanium source [64–66].

2.2.1. Monovacant Keggin unit-silica/titania composite films ($[X^{n+}W_{11}O_{39}]^{(12-n)-}/SiO_2(TiO_2)$, X = Si, Ge or P)

The $[X^{n+}W_{11}O_{39}]^{(12-n)-}/SiO_2(TiO_2)$ film was prepared according to the following three steps [64,65]. First, preparation of $[X^{n+}W_{11}O_{39}]^{(12-n)-}/SiO_2(TiO_2)$ sol via hydrolysis of $Si(OC_2H_5)_4$ or $Ti(OC_4H_9)_4$ at pH 1.5 in the presence of $[X^{n+}W_{11}O_{39}]^{(12-n)-}$; second, coating of the sol on a quartz slide by high-speed spinning; finally, calcination of the slide at different temperatures.

Formation of the $[X^{n+}W_{11}O_{39}]^{(12-n)-}/SiO_2(TiO_2)$ hybrid materials is based on the following two facts. First, 1:11 series of polyoxotungstates $[X^{n+}W_{11}O_{39}]^{(12-n)-}$ (X = P, Si, Ge), are the monovacant derivatives of the saturated Keggin anion, $[X^{n+}W_{12}O_{40}]^{(8-n)-}$. As removal of tungsten–oxygen octahedral from a saturated Keggin anion framework leads to increase and localization of the anionic charge, the resulting lacunary anion becomes highly nucleophilic and reacts easily with electrophilic groups. Second, hydrolysis of $Si(OC_2H_5)_4$ or $Ti(OC_4H_9)_4$ under acidic condition yields the sol of $Si(OSi)_x(OH)_{4-x}$ or $Ti(OTi)_x(OH)_{4-x}$ ($x = 0-4$). These products construct the silica (titania) network via dehydration, and the network has the electrophilic surface silicon or titanium atoms in the surface hydroxyl groups of the anatase TiO_2 or SiO_2 network, which demonstrate chemical reactivity toward lacunary Keggin units. Therefore, the $[X^{n+}W_{11}O_{39}]^{(12-n)-}/SiO_2(TiO_2)$ hybrid silica (titania) materials formed via W–O–Si(Ti) bridges. That is $[X^{n+}W_{11}O_{39}]^{(12-n)-}$ in the $[X^{n+}W_{11}O_{39}]^{(12-n)-}/SiO_2(TiO_2)$ composites presented one vacant site, which allowed to connect two $SiO_4(TiO_4)$ units in the silica (titania) network to make up one tungsten–oxygen octahedral lacuna, and the terminal nucleophilic oxygen atom in pure $[X^{n+}W_{11}O_{39}]^{(12-n)-}$ became a bridge atom due to connecting the electrophilic silicon or titanium atom in hydroxyl groups, therefore, W–O–Si(Ti) bridges were formed. Appearing new and strong IR adsorption peak at *ca.* 970 cm^{-1} evidenced that the W–O–Ti covalent bond was formed in as-prepared composite films [43]. In addition, changes were observed in their UV absorption spectra due to the structures of the Keggin anions in the films tending to saturation after chemical bonding with the SiO_4 units in the silica network. That is, the oxygen-to-tungsten charge-transfer (OMCT) band at W–O–W bond of $[X^{n+}W_{11}O_{39}]^{(12-n)-}$ changed from relatively plat to steep [64]. It must be emphasized that this saturation does not mean the transformation from 1:11 to 1:12.

2.2.2. Lacunary Keggin-type polyoxometalate-based highly ordered macroporous composite films ($[X^{n+}W_{11}O_{39}]^{(12-n)-}$-$MO_2$, X = P, Si, Ge; M = Si, Ti)

In the past few years, a great deal of attention has been paid to the fabrication of highly ordered porous materials due to their potential for wide practical applications in separation processes, large-molecule catalysis, host–guest systems, thermal or electrical insulators and semiconductor oxides with tunable band gaps [67,68]. Especially, films with interconnected highly ordered pores have also been extensively studied because of their wide applications in separations, catalysis, optical information processing, and microwave shielding [69,70]. Methods developed to fabricate porous films include CVD, electrochemical deposition, hydrodynamic infiltration of nanoparticles, selective etching, self-assembly of block copolymers, and replica molding against templates [71,72]. Among these methods, colloids are first crystallized as a template and then porous structures are formed via a replication process, which is an easy and efficient method [73].

We have reported a kind of highly ordered macroporous composite film with the composition of $[X^{n+}W_{11}O_{39}]^{(12-n)-}$-$MO_2$ (X = P, Si, Ge; M = Si, Ti) [66]. Method of the fabri-

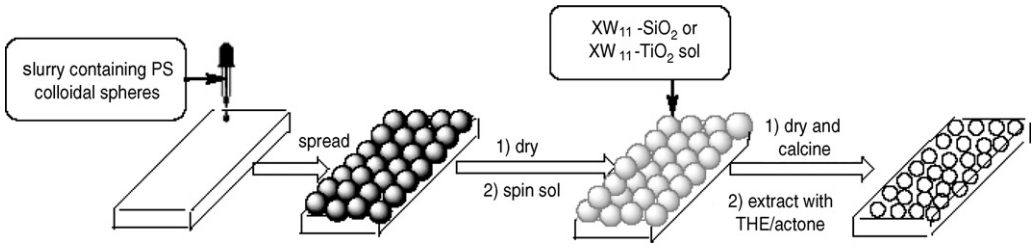

Scheme 2. The sketch map of the reaction progress of preparation of macroporous $[X^{n+}W_{11}O_{39}]^{(12-n)-}$-$MO_2$ composite films (X = P, Si, Ge; M = Si, Ti). $[X^{n+}W_{11}O_{39}]^{(12-n)-}$ was abbreviated XW_{11}.

cation of this film was simple and easily handled, including polystyrene (PS) templating sol–gel as well as spin coating (Scheme 2). At first, monodispersed colloidal PS particles were first assembled on quartz slides by utilizing capillary force. Afterwards $[X^{n+}W_{11}O_{39}]^{(12-n)-}$-$MO_2$ sol was infiltrated into the voids between these template PS spheres on the slides by a spin-coating technique. After the composite films were dried at room temperature, PS spheres were removed by extraction with tetrahydrofuran/acetone in ultrasonic generator, resulting in highly ordered macroporous $[X^{n+}W_{11}O_{39}]^{(12-n)-}$-$MO_2$ composite films. The reason of selecting lacunary Keggin-type POMs as the precursors was that the covalent bond between the POM unit and MO_2 matrix can also be formed. The adsorption peak of the film at *ca.* 970 cm^{-1} (stretching vibration of W–O–Ti bond) was also detected and the detected ^{31}P MAS NMR resonance signal for the PW_{11}-SiO_2 and PW_{11}-TiO_2 film was −13.5 and −14.2 ppm, respectively [66], further confirming the incorporation of the Keggin unit into the SiO_2 or TiO_2 matrix, and the structure of the monovacant Keggin unit in the composite film tended to becoming saturated due to grafting silanol groups or hydroxyl groups of titania from the matrix network into its vacant sites (^{31}P MAS NMR resonance signal for $[PW_{12}O_{40}]^{3-}$ and $[PW_{11}O_{39}]^{7-}$ was −14.9 and −10.4 ppm, respectively [74]).

3. Properties

3.1. Optical absorption property

The optical absorption property of the photocatalytic materials is one of the most important factors to affect their photocatalytic activity. In metal oxide particulates, atomic orbitals coalesce to form energy bands. Incident light (λ) higher than the band gap energy of the semiconductor (E_g) leads to separation of the electron and hole and then initiates the chemical reaction. Similarly, excitation of the OMCT band of the polyoxotungstate cluster in the near UV-light region results in the charge transfer from an O^{2-} ion to a W^{6+} ion occurred at W–O–W bonds, leading to the formation of a pair of hole center (O^-) and trapped electron center (W^{5+}). The process is described in Eq. (1):

$$[W^{6+}\text{–}O^{2-}\text{–}W^{6+}] \xrightarrow{h\nu} [W^{5+}\text{–}O^{-}\text{–}W^{6+}] \quad (1)$$

The band gap energy refers to the energy difference between the valence band and conduction band for semiconductor, as for the polyoxotungstate, it refers to the energy difference between the HOMO and LUMO. The band gap energy can be calculated from the absorption spectrum of the materials. The higher the band gap energy, the higher excitation energy is needed to excite the electron from the valence band (HOMO) to conduction band (LUMO).

For the silica supported POM powder or film, their peak position of the OMCT band was in agreement with that of the starting POM, and the band was not interfered with the silica matrix (Fig. 2a and c). Absorption at *ca.* 200 and 250 nm is attributed to charge-transfer from an O^{2-} ion to a W^{6+} ion in the Keggin unit at W=O and W–O–W bonds, respectively. In the case of $[M(H_2O)PW_{11}O_{39}]^{5-}$, another wide absorption peak ranged from 500 to 650 nm is due to d–d transition typical for octahedral M^{2+} with six oxygen bond ligands. However, as for the titania supported POMs, their absorption band is different from that of the starting POM or the titania matrix, *i.e.*, the OMCT band (charge transfer from O 2p to W 5d for POM and O 2p to Ti 3d for titania, respectively) originated from the starting Keggin (or Dawson) unit or titania matrix disappeared, whereas a new broad peak appeared with red-shift absorption band and the absorption threshold onset that continuously extended to the visible region (Fig. 2b, d and e). This new absorption band corresponded to relatively low band gap energy. Silica is photoinactive, and its electronic attributes is very different from that of the polyoxotungstate, therefore, it do not interfere with the optical absorption property of the polyoxotungstate after formation of the polyoxotungstate–silica composite. In the case of the polyoxotungstate–anatase TiO_2 composite, the TiO_2 support has the similar electronic attributes with those of the polyoxotungstate, therefore, the presence of the Keggin or Dawson unit has an influence on the electronic properties of anatase TiO_2. Similar energy levels of Ti 3d and W 5d would suggest that the POM incorporation into an anatase framework only produced moderate widening of electronic absorption band (similar crystal field splitting for both cations, just slightly differing in the d orbital average size). Red-shift of the OMCT band indicates that there is a doping energy level between the conduction bands and valence bands of TiO_2, and the electronic properties of the composites resulted from the following two transition forms, *i.e.*, the transition from the valence band to the conduction band (corresponding to wide band gap), and the transition from the valence band to the doping energy level (corresponding to narrow band gap energy) [49].

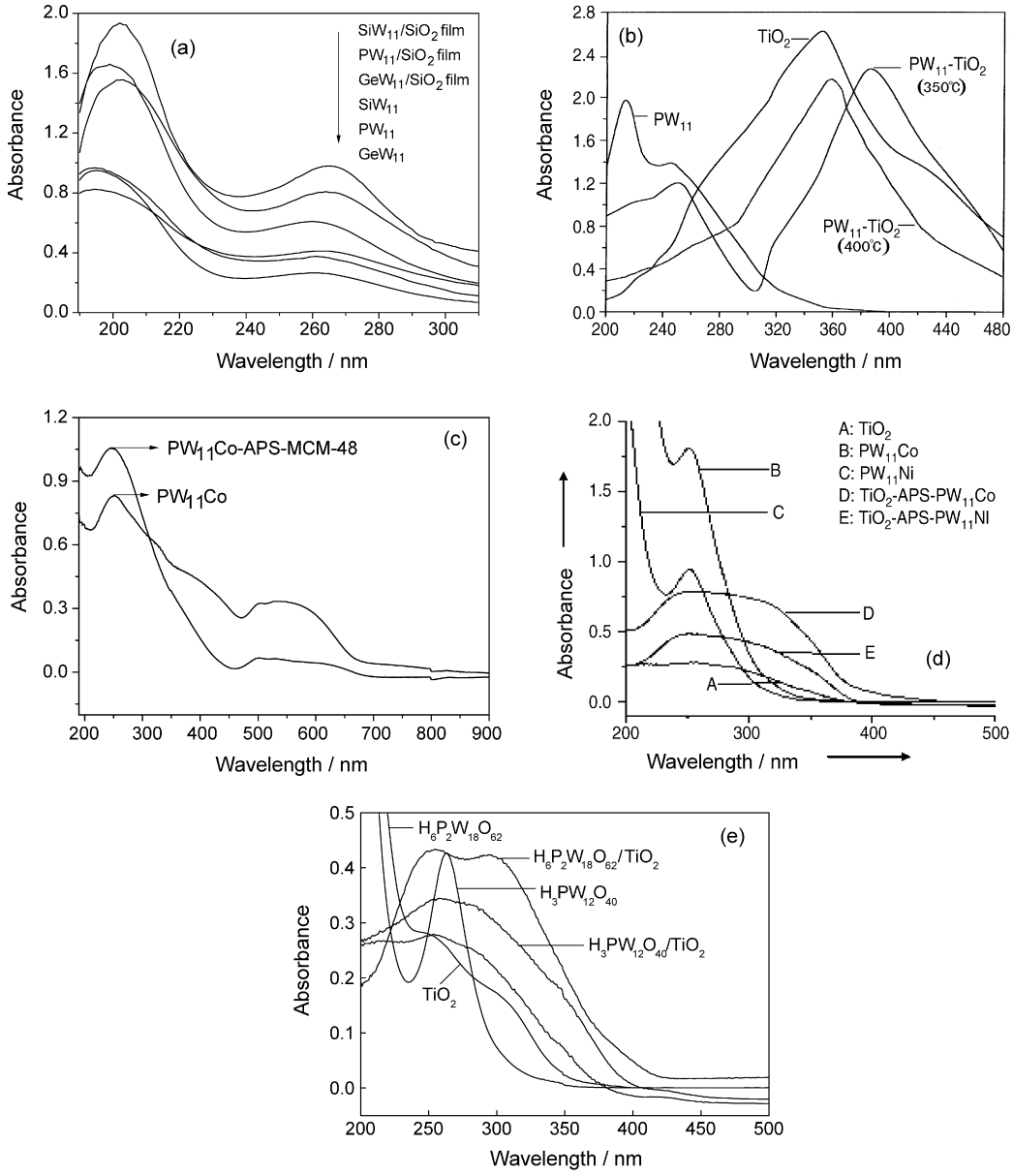

Fig. 2. UV diffuse reflectance spectra (UV/DRS) of the solid POMs: (a) starting XW_{11} and their corresponding XW_{11}/SiO_2 composite films. X = Si, Ge, P $[X^{n+}W_{11}O_{39}]^{(12-n)-}$ was abbreviated XW_{11}; (b) starting PW_{11}, pure TiO_2, and corresponding PW_{11}/TiO_2 films prepared at different calcination temperature (350, 400 °C), $PW_{11}O_{39}{}^{7-}$ was abbreviated PW_{11}; (c) $PW_{11}Co$ and $PW_{11}Co$-APS-MCM-48, $[Co(H_2O)PW_{11}O_{39}]^{5-}$ was abbreviated $PW_{11}Co$; (d) $PW_{11}Co(Ni)$ and $PW_{11}Co(Ni)$-APS-TiO_2; (e) anatase TiO_2, starting $H_3PW_{12}O_{40}$ or $H_6P_2W_{18}O_{62}$, and the corresponding anatase TiO_2 supported Keggin or Dawson unit.

3.2. Surface textural property

Surface textural property of the above described POM-containing composite photocatalyst powder was characterized by the nitrogen adsorption–desorption analysis, and the results were summarized in Table 1, in addition, the representative nitrogen adsorption–desorption isotherm and pore-size distribution were showed in Fig. 3. Compared with the starting POM, the BET surface area was improved after formation of the composite catalysts. In the case of $[M(H_2O)PW_{11}O_{39}]^{5-}$-APS-MCM-48 or $[M(H_2O)PW_{11}O_{39}]^{5-}$-APS-$TiO_2$, the isotherms of Type IV (IUPAC definition) were observed with steep hysteresis loop at a relative pressure from 0.4 to 0.8 [52,75]. Compared with the mesoporous MCM-48 support, both of the BET surface areas and the pore volume of the composites reduced greatly after formation of the $[M(H_2O)PW_{11}O_{39}]^{5-}$-APS-MCM-48 composites. This may be due to the fact that introduction of the organic groups and large Keggin unit blocked the pores of MCM-48. At the same time, the pore size of the composites was enlarged, *i.e.*, 5.4 nm for the $PW_{11}Co$-APS-MCM-48 and 5.8 nm for the $PW_{11}Ni$-APS-MCM-48, respectively. The most likely reason for these changes is that grafting large Keggin unit to the APS-functionalized MCM-48 support destroyed the cubic structure of the MCM-48, resulting in changes of pore sizes. XRD pattern showed that the cubic phase of the MCM-48 was totally destroyed after formation of $PW_{11}Co/Ni$-

Table 1
Surface textural property of the POM-containing composite photocatalyst powders

Catalyst	SA[a] (m^2/g)	PD[b] (nm)	PV[c] (cm^3/g)
$H_3PW_{12}O_{40}/TiO_2$	201.2	0.60/4.0	0.14
$H_6P_2W_{18}O_{62}/TiO_2$	193.4	0.61/4.0	0.21
$[Co(H_2O)SiW_{11}O_{39}]^{6-}$-APS-MCM-48	170.6	5.4	0.24
$[Ni(H_2O)SiW_{11}O_{39}]^{6-}$-APS-MCM-48	158.3	5.8	0.29
$[Ni(H_2O)PW_{11}O_{39}]^{5-}$-APS-$TiO_2$	56.8	36.0	0.17
$[Co(H_2O)PW_{11}O_{39}]^{5-}$-APS-$TiO_2$	68.3	33.8	0.13

[a] BET surface area.
[b] Average pore diameter.
[c] BJH average pore volume.

APS-MCM-48 composite, and the products were amorphous. Formation of the mesopores of the $[M(H_2O)PW_{11}O_{39}]^{5-}$-APS-MCM-48($TiO_2$) is due to the aggregation among the particles [52].

Very interestingly, anatase TiO_2 supported Keggin or Wells-Dawson unit, $H_3PW_{12}O_{40}/TiO_2$ or $H_6PW_{18}O_{62}/TiO_2$, exhibited bimodal pore systems (micro-mesoporosity) with pore size at *ca*. 0.6 and 4.0 nm, respectively (Fig. 3). The curves showed two well-defined adsorption steps. At first, at very low relative pressure ($p/p_0 < 0.1$), the amount of volume adsorbed increased rapidly, indicating that the powders contain micropores (Type I). In addition, the *t*-plot does not cross through zero, further suggesting some micropores existed in the composite. Second, at an intermediate relative pressure ($p/p_0 = 0.4$–0.8), the curves exhibit a hysteresis loop, indicating that the powders contain mesopores (Type IV). According to Kumar et al. [76] and Yu et al. [77], formation of this bimodal pore-size distribution is due to hard aggregates in the powders. There are two types of pores in the bimodal pore size distribution. One is the finer intraaggregated pore, corresponding to micropores, and the other is the larger interaggregated pore, corresponding to mesopores. These aggregatings occurred during the preparation process of the composite catalyst.

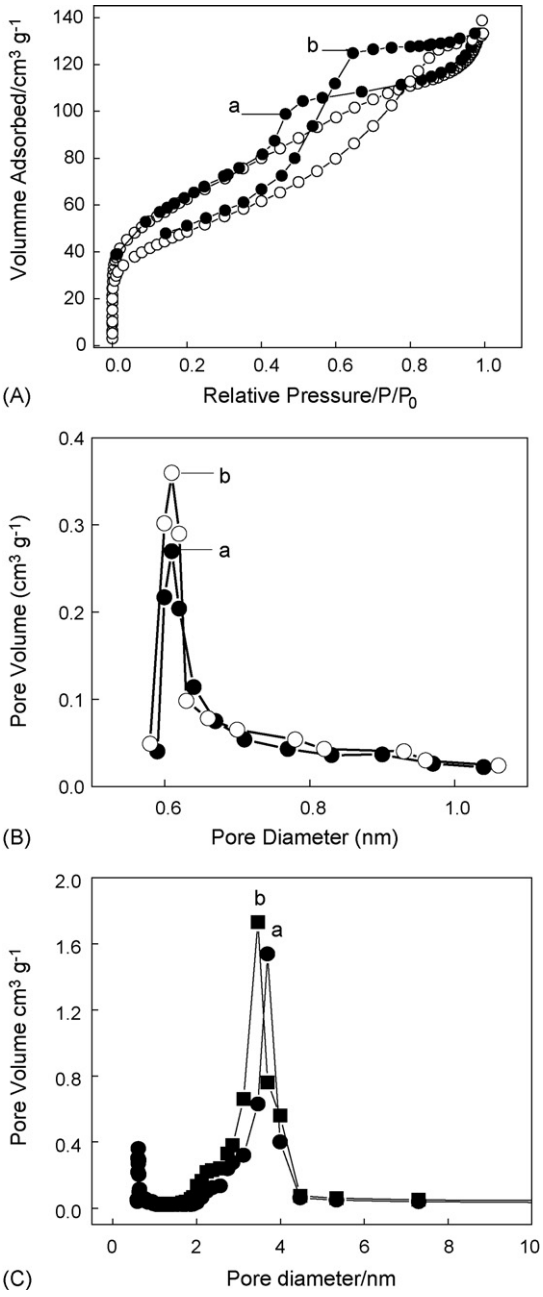

Fig. 3. (A) Nitrogen adsorption–desorption isotherms, (B) and (C) BJH pore size distributions for micropores and mesopores. (a) $H_3PW_{12}O_{40}/TiO_2$ and (b) $H_6P_2W_{18}O_{62}/TiO_2$.

3.3. Morphology

The particles of titania or APS-silica supported POM powders described above were sphere-like and exhibited uniform size distribution with the average size of smaller than 10 nm, and aggregation among particles was also observed (Fig. 4A–C). The rings recorded from the selected area electron diffraction (SAED) of the $H_3PW_{12}O_{40}/TiO_2$ were indexed to diffraction from the (1 0 1), (0 0 4), (2 0 0), (1 0 5), (2 0 4), (1 1 6), and (2 1 5) planes of anatase (Fig. 4A). As for the POM–silica (titania) composite film, the surface morphology of the films were uniform with the thickness of *ca*. 300 nm for $SiW_{11}O_{39}^{8-}/SiO_2$ and 500 nm for $PW_{11}O_{39}^{7-}/TiO_2$, respectively, estimated from the edge of the visible crack (Fig. 4D and E). In the case of macroporous $PW_{11}O_{39}^{7-}/TiO_2$ film (Fig. 4F), the pores were observed with the average size of 350 nm.

4. Heterogeneous photocatalysis applications

The above described POM-containing composites exhibited one or more advantages including nanometer sizes, lower band gap energy than the starting POM or anatase TiO_2 matrix, synergistic effect, unique surface physico-chemical properties, and easily handled for recycle applications, therefore, they are the good candidates of the heterogeneous photocatalytic materials.

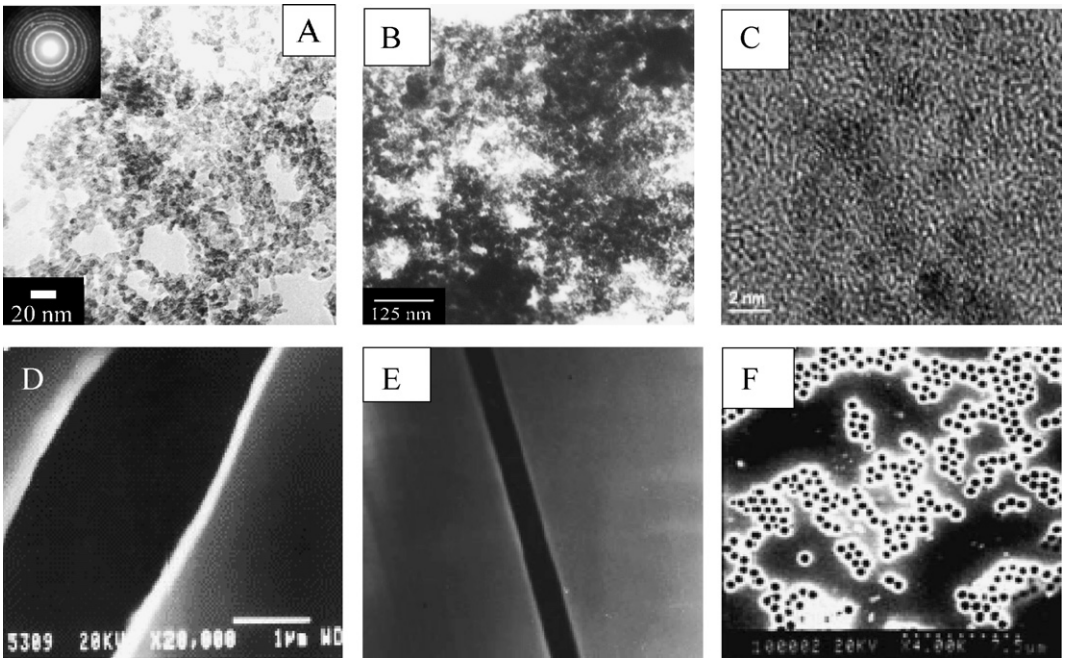

Fig. 4. TEM images of the $H_3PW_{12}O_{40}/TiO_2$ (A), PW_{11}Co-APS-MCM-48 (B), and $H_5FeW_{12}O_{40}\cdot 10H_2O$/silica structured fabrics (C). SEM images of the composite films: $SiW_{11}O_{39}^{8-}/SiO_2$ (D), $PW_{11}O_{39}^{7-}/TiO_2$ (E), and 3DOM $PW_{11}O_{39}^{7-}/TiO_2$ (F).

4.1. Visible-light photocatalytic activity of the bimodal porous $H_3PW_{12}O_{40}/TiO_2$ and $H_6PW_{18}O_{62}/TiO_2$

Parathion-methyl, a kind of chemically stable organophosphorus pesticide that is widely used in agriculture recently, and dyes with different structures including either azoic [congo red (CR), methyl orange (MO), ponceau G (PG), orange II (OII), and eriochrome blue black B (EB)], anthraquinonic [alizarin S (AS)], heteropolyaromatic [methylene blue (MB)], fluorescent [neutral red (NR), rhodamine B (RB)], and sulfonic [fuchsin acid (FA)] were selected as the targets to study the visible-light photocatalytic activity of as-prepared bimodal porous $H_3PW_{12}O_{40}/TiO_2$ and $H_6PW_{18}O_{62}/TiO_2$. The light source selected was a 400 W Xe lamp, and the lamp was surrounded by an optical glass jacket, therefore, the emission rays below 410 nm were almost filtered.

Direct photolysis of an aqueous parathion-methyl (50 mg L^{-1}) under visible-light irradiation for 4 h did not cause any changes of its concentration. In addition, in the homogeneous system of an aqueous parathion-methyl/$H_3PW_{12}O_{40}$ or $H_6P_2W_{18}O_{62}$, degradation of parathion-methyl was hardly observed after visible-light irradiation for 4 h. The photocatalytic activity of Degussa P-25 was low under the same conditions, while as-prepared nanosize anatase TiO_2 totally adsorbed the reactant molecules during the adsorption process. Whereas, the concentration of the parathion-methyl in the reaction system decreased rapidly by using $H_3PW_{12}O_{40}/TiO_2$ or $H_6P_2W_{18}O_{62}/TiO_2$ as the visible light-driven-photocatalyst, and it only needed *ca*. 40 min to completely destruct it (Fig. 5a). At the same time, some intermediates including acetic acid and formic acid were detected in this system, and total disappearance of acetic acid and formic acid needed 120 and 160 min, respectively, by using the $H_3PW_{12}O_{40}/TiO_2$ as a photocatalyst.

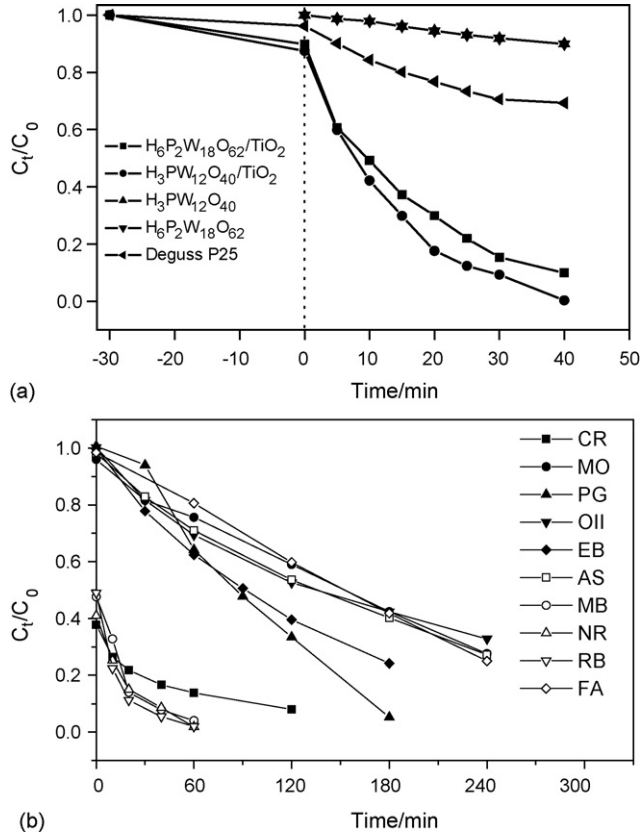

Fig. 5. (a) Photocatalytic degradation of an aqueous parathion-methyl ($c_0 = 50$ mg L^{-1}; 120 mL) under visible-light excitation. Each photocatalyst used was 0.2 g, and c_t refers to the concentration of parathion-methyl in the reaction system at t time; (b) Photocatalytic degradation of dyes ($c_0 = 50$ mg L^{-1}; 120 mL) by visible-light irradiation of the $H_3PW_{12}O_{40}/TiO_2$ (0.25 g).

The final products yielded during photodegradation of the parathion-methyl should be NO_3^-, SO_4^{2-}, and PO_4^{3-}, respectively, but only NO_3^- and SO_4^{2-} ions were detected. This may be due to the fact that highly charged PO_4^{3-} ion strongly adsorbed on the surface of the nanoscale photocatalyst. This adsorption also led to hardly determining the concentration of NO_3^- or SO_4^{2-} ion quantitatively and accurately, and the estimated yield for NO_3^- and SO_4^{2-} ion was *ca.* 88 and 71% [49], respectively. The overall photodecomposition reaction is shown in Eq. (2)

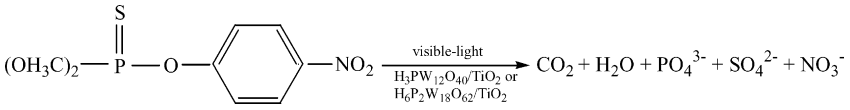

(2)

Bimodal porous $H_3PW_{12}O_{40}/TiO_2$ also exhibited much higher visible-light photocatalytic activity to degrade various dyes including extremely stable azoic dyes and heteropolyaromatic dyes (Fig. 5b). That is, the concentrations of CR, MB, NR, and RB decreased by *ca.* 50% after stirring the suspension of an aqueous dye and the $H_3PW_{12}O_{40}/TiO_2$ in the dark for 30 min, suggesting that the strong adsorption of the reactant molecule occurred on the surface of the catalyst and resulting in the higher conversion in the shorter reaction time. The adsorption of other dyes (MO, PG, OII, EB, AS, and FA) was weaker on the surface of the $H_3PW_{12}O_{40}/TiO_2$, and the conversion was lower accordingly. During the process of the dye adsorption on the surface of the catalyst in the dark, the colors of the dyes changed, suggesting formation of preassociated complex between the $H_3PW_{12}O_{40}/TiO_2$ and the dye, which is an important factor to ensure high photocatalytic activity of the $H_3PW_{12}O_{40}/TiO_2$. In general, the higher the conversion, the faster the initial reaction rate is. But the conversion of CR is high, and its initial reaction rate is slow. It was possible because the CR molecule has large and complicate structure, and its degradation is difficult in this system [48].

4.2. UV-light photocatalytic activity of amine-functionalized mesoporous silica/anatase titania impregnated with TMSP

4.2.1. $[M(H_2O)PW_{11}O_{39}]^{5-}$-APS-$TiO_2$

$[M(H_2O)PW_{11}O_{39}]^{5-}$-APS-$TiO_2$ (M = Co/Ni) did not exhibited visible-light photocatalytic activity to dye degradation although the composites possessed anatase phase structure and relatively narrow band gap energy (Fig. 2d). And degradation of dyes (CR, MO, AS and NR) or organochlorine pesticide (HCB) was performed under the near-UV light irradiation [51]. The results showed that complete degradation of a trace HCB (2 mg L^{-1}) in aqueous solution was achieved after 40 min UV-light irradiation of the $[M(H_2O)PW_{11}O_{39}]^{5-}$-APS-$TiO_2$ (Fig. 6a). In addition, disappearance of CR, MO, and NR (50 mg L^{-1}) was significantly fast, and they were destructed totally after only *ca.* 40 min UV-light irradiation of the suspension including an aqueous dye and the $[M(H_2O)PW_{11}O_{39}]^{5-}$-APS-$TiO_2$ (Fig. 6b). Moreover, the photocatalytic activity of the $[Co(H_2O)PW_{11}O_{39}]^{5-}$-APS-$TiO_2$ was very similar to that of the $[Ni(H_2O)PW_{11}O_{39}]^{5-}$-APS-$TiO_2$, and they all exhibited much higher UV-light photocatalytic activity than that of as-prepared anatase TiO_2.

4.2.2. $[M(H_2O)PW_{11}O_{39}]^{5-}$-APS-MCM-48

RB, HCB, and parathion-methyl were chosen as the model molecules to investigate the UV-light photocatalytic activity of the $[M(H_2O)PW_{11}O_{39}]^{5-}$-APS-MCM-48 (M = Co/Ni). The results showed that the $[M(H_2O)PW_{11}O_{39}]^{5-}$-APS-MCM-48 exhibited higher activity than that of the homogeneous $[M(H_2O)PW_{11}O_{39}]^{5-}$ for degradation of the above three model molecules, and total disappearance of RB, HCB, and parathion-methyl needed 120, 60, and 30 min, respectively, under near-UV light irradiation of the suspension including an aqueous organic pollutant and the $[M(H_2O)PW_{11}O_{39}]^{5-}$-APS-MCM-48. In addition, the photocatalytic activity of the

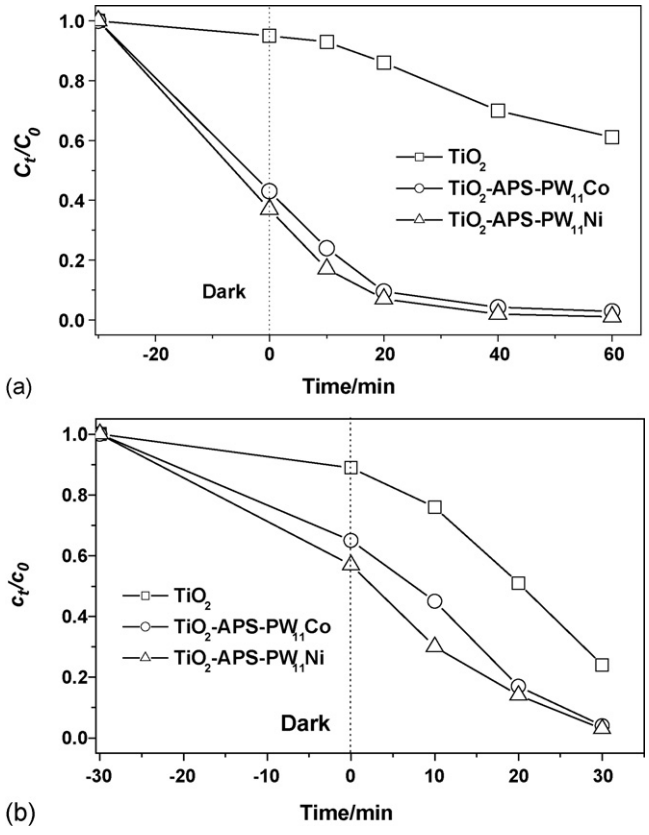

Fig. 6. (a) Concentration of HCB changes as a function of UV-light irradiation time (c_0 = 2 mg L^{-1}; 80 mL; weight of catalyst 0.1 g) and (b) concentration of MO changes as a function of UV-light irradiation time (c_0 = 50 mg L^{-1}; 80 mL; weight of catalyst 0.1 g).

$[Co(H_2O)PW_{11}O_{39}]^{5-}$-APS-MCM-48 was very similar to that of the $[Ni(H_2O)PW_{11}O_{39}]^{5-}$-APS-MCM-48 [52].

4.3. UV-light photocatalytic activity of the polyoxometalate-containing composite films

4.3.1. $[X^{n+}W_{11}O_{39}]^{(12-n)-}/SiO_2$ film

The model reaction selected was degradation of an aqueous formic acid into CO_2 and H_2O. Formic acid is an organic pollutant existed in the industrial wastewater or a stable intermediate found in various photodegradation processes. Studies showed the $[X^{n+}W_{11}O_{39}]^{(12-n)-}/SiO_2$ films (X = Si, Ge, or P) exhibited activity to formic acid (4 mmol L^{-1}) degradation under UV-light irradiation, *i.e.*, the conversion of formic acid into CO_2 and H_2O was in the range of 50–60% after UV-light irradiation of the different slides for 120 min, while the conversion of formic acid was only 6.5% under the same conditions except that as-prepared silica film was used [64]. The rate constant for the three films was similar, suggesting that the reaction rate of the $[X^{n+}W_{11}O_{39}]^{(12-n)-}/SiO_2$ film-photocatalyzed formic acid degradation was similar although the central atoms (Si, Ge, or P) in the selected Keggin units are different. However, it was difficult to compare the photocatalytic activity of three as-prepared films precisely owing to the different preparation experiment conditions used. Compared with the powder heterogeneous POM-containing photocatalytic materials, the films have the advantage of more easily handling for recycling uses, and the leakage of the $[X^{n+}W_{11}O_{39}]^{(12-n)-}$ from the silica matrix was hardly observed during three catalytic runs, suggesting that the films had a high stability in an aqueous solution.

4.3.2. $PW_{11}O_{39}^{7-}/TiO_2$ film

The photocatalytic activity of the $PW_{11}O_{39}^{7-}/SiO_2$ film was attempted to be improved by representing silica matrix for photoactive titania support. For this purpose, the $PW_{11}O_{39}^{7-}/TiO_2$ film was prepared. Calcination of the $PW_{11}O_{39}^{7-}/TiO_2$ film at 350 °C resulted in mainly anatase phase structure of TiO_2, and the film thus obtained exhibited higher photocatalytic activity to CR (30 mg L^{-1}) degradation than that of as-prepared pure TiO_2 or $[X^{n+}W_{11}O_{39}]^{(12-n)-}/SiO_2$ film [65]. At lower calcination temperature (<350 °C), only a little amount of anatase phase in the film was formed, therefore, the photocatalysis originated from the anatase TiO_2 did not well developed. At higher calcination temperature (*e.g.*, 400 °C), lots of the $PW_{11}O_{39}^{7-}$ cluster on the films was destroyed and transformed to WO_3 phase, meanwhile, most of the anatase phase was transformed to rutile phase, resulting in obvious decrease of the photocatalytic activity of the film. Evolution of some intermediates (acetic acid and formic acid) and final products (NH_4^+, SO_4^{2-}, NO_2^-, and NO_3^-) were detected, indicating that both degradation and mineralization occurred during the process of UV-light irradiation of the film and CR solution. The overall photodecomposition reaction is shown in Eq. (3)

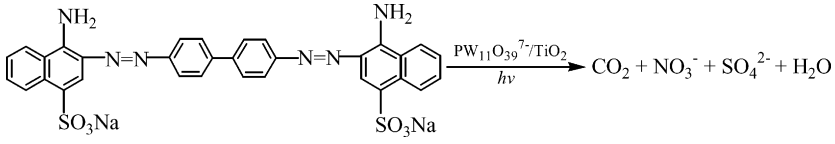

(3)

4.4. Mechanism studies

Generally, the solid POMs on excitation with near UV- or visible-light served as photocatalysts follow a variety of similar processes with those of the metal oxide particles in heterogeneous systems [17]. Prior to photoactivation, preassociated complex or preassociation equilibrium was formed during the substrate adsorption process in the dark, for that matter, a supramolecular species [*i.e.*, POM/EO_2-substrate in Scheme 3A(a)] between the photocatalyst and substrate yielded, which can be confirmed by the electronic spectroscopy (OMCT band shifted), NMR data, X-ray data or kinetic evidence [17,31].

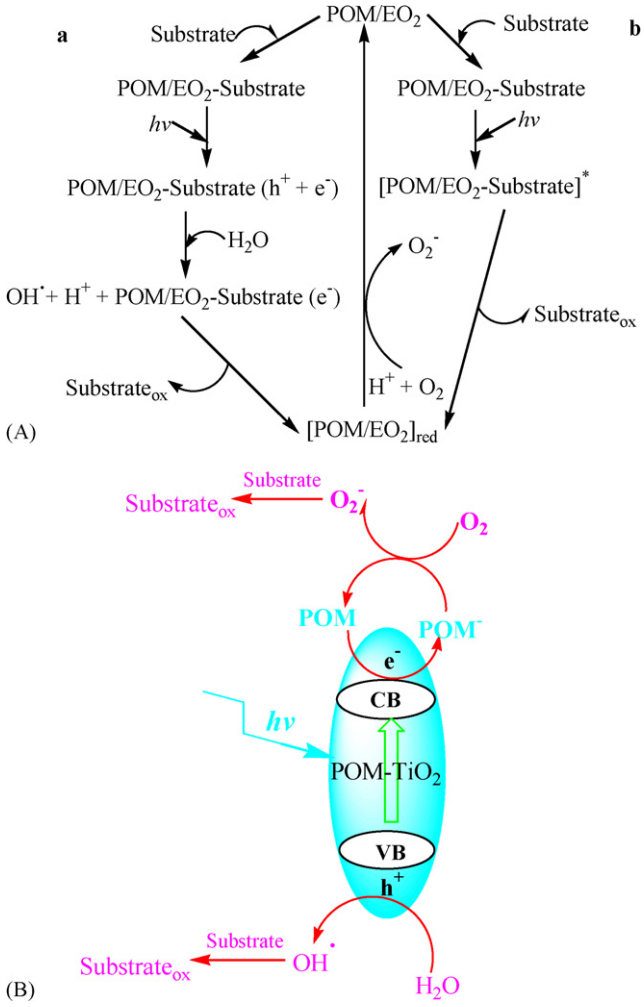

Scheme 3. Proposed photocatalytic cycle of the supported POM composite. (A) EO_2 support is photoinactive. Path (a) represents the photooxidation of the organic compounds through OH radicals. Path (b) represents direct reaction of the excited POM catalyst with the substrate. (B) The support is photoactive anatase TiO_2.

In all studies, high affinity of the organic compounds for the POM has been observed. Afterwards, the catalyst was activated by incident light energy higher than the energy bands of POM, which led to the charge transfer from an O^{2-} ion to a W^{6+} ion at W–O–W bonds and formation of a strongly oxidizing excited state of POM [*i.e.* [POM/EO_2-substrate]* in Scheme 3A(a), or POM/EO_2-substrate ($h^+ + e^-$) in Scheme 3A(b)], with reduction potentials exceeding 2.5 V versus the NHE for many POMs [18,78], thus, a pair of the hole center (O^-) and trapped electron center (W^{5+}) formed. Photooxidation of the organic compounds (electron donors) was performed via the reaction through OH radicals (path (a) in Scheme 3A) and direct reaction of the excited POM catalysts with the substrate (path (b) in Scheme 3A). The "surface" bound OH radicals were produced by the reaction of the excited catalyst with water (*i.e.*, oxidative hole trapping). The following observations substantiate the formation of the OH radicals: (i) OH adducts (hydroxylation products) have been detected in the photolysis experiments with aromatic hydrocarbons in the presence of POM [17,41,45]; (ii) ESR trapping experiments had detected OH radicals upon photolysis the organics in the presence of POM [79]; (iii) the generation of OH radicals is also suggested by the fact that the excited state potentials of most POM are more positive than that given in Eq. (4) [17].

$$OH + H^+ + e^- \rightarrow H_2O, \qquad E = 1.90\,V \quad \text{versus} \quad NHE \tag{4}$$

Finally, reoxidation of the POM catalyst (*i.e.* [POM/EO_2-substrate]$_{red}$) to its original oxidation state was easily performed by an electron acceptor such as dioxygen dissolved in the suspension. The rate-determining step in the photocatalytic cycle has been reported to be the reoxidation of the catalyst [17]. Having undergone the above steps, a net photocatalytic cycle was completed. The reoxidized form of POM was then capable of engaging in another series of electron transfers that may continue until the reactant finished.

However, as for the anatase TiO_2-supported POM photocatalysts, the photoreaction mechanism is a little different from that described above, and the synergistic effect occurred between the POM unit and TiO_2 support during the POM/TiO_2 photocatalysis process. That is, anatase TiO_2 is photoactive, while POM has empty d orbits. POM can be used as a good electron acceptor that can store several electrons per molecule [80]. After addition of homogeneous POM into the TiO_2 photocatalytic systems, the fast charge-pair ($h^+ - e^-$) recombination on the surface of TiO_2 can be retarded effectively. This is due to the fact that POM has the ability to enhance the transfer rate of the electrons in conduction band (CB) by accepting e^- (photogenerated electrons) to its empty d orbits, therefore, the trapped holes (h^+) have sufficient time to react with the surface water molecule to produce OH radicals. Several research groups have studied this synergistic effect. Ozer and Ferry [31] had reported that significant rate enhancement for 1,2-dichlorobenzene photooxidation was obtained after addition of aqueous POM anions such as $PW_{12}O_{40}{}^{3-}$, $SiW_{12}O_{40}{}^{4-}$, or $W_{10}O_{32}{}^{4-}$ into the TiO_2 suspensions. Ryu and Choi [81] had reported that addition of homogenous $SiW_{12}O_{40}{}^{4-}$ into the naked TiO_2 suspension greatly increased the photocatalytic oxidation rate of As (III) to As (V), and the latter is less toxic and less mobile in the aquatic environment. And they pointed out that the presence of POM enhanced the opportunity of generation of superoxides, which are the main oxidant of As (III). Park and Choi [82] also had proved this synergistic effect through photoelectrochemical investigation, and they concluded that POM successfully transferred CB electrons on TiO_2 particles to an inert collector electrode with generating photocurrents under UV-light illumination. The magnitude of photocurrent was directly proportional to the reduced POM concentration and markedly decreased in the presence of dissolved O_2 due to the rapid reoxidation of the reduced POM by it. Combination of the above reports and our research results, the proposed photocatalytic cycle of the POM/TiO_2 composite (anatase phase) is shown in Scheme 3B. It can be reasonably concluded that the role of the POM in TiO_2 photocatalysis is critical in enhancing the overall photoefficiency by retarding the fast recombination of charge-pair ($h^+ - e^-$) on TiO_2 and producing strong oxidant, $O_2{}^{\bullet -}$, a kind of main oxidant of the substrate except $OH^\bullet$ radicals [81].

Otherwise, similar energy levels of Ti 3d (for anatase TiO_2) and W 5d (for POM) suggested that the POM cluster incorporation into the anatase framework only produced moderate widening of electronic band, accordingly, the OMCT band of TiO_2 was redshifted and its band gap energy was decreased [49]. Therefore, the energy of the electron transition from the valence band to the doping energy level or from the doping energy level to the conduction band level was lower than that of the valence band to the conduction band of TiO_2, resulting in more photogenerated electrons and holes to participate in the photocatalytic reactions. This is the most important factor to enhance the photocatalytic activity of TiO_2 or POM, making it possible to utilize visible-light-type excitation more efficiently than classic Ti-only based one (see results of Fig. 5 and Refs. [48,49,83]) or improving the photocatalytic activity obviously compared with that of the homogeneous POM or as-prepared anatase TiO_2 (see results of Fig. 6 and Ref. [51]).

The porous structure of as-prepared composites also played an important role to enhance their photocatalytic activity. The BET specific surface area of the porous POM-containing composites is largely increased. This greater surface area results in an increase in the photocatalytic activity of POMs by providing more contact areas between the catalyst and the substrate for the surface-mediated electron-transfer reactions to take place [31]. In addition, the porous catalysts show a strong adsorption to the substrates, which is also benefit to enhance the activity of POM since the adsorption is the first step of the photocatalytic reaction. This adsorption was obviously observed in the POM/TiO_2 or $[M(H_2O)PW_{11}O_{39}]^{5-}$-APS-$TiO_2$($SiO_2$)-photocatalyzed organic degradation reactions (Figs. 5 and 6). The above discussion showed that the positions of the OMCT band for the bimodal porous $H_3PW_{12}O_{40}$/TiO_2 and mesoporous $[M(H_2O)PW_{11}O_{39}]^{5-}$-APS-$TiO_2$ were very close, however, only the $H_3PW_{12}O_{40}$/TiO_2 exhibited visible-light photocatalytic activity to dyes and parathion-methyl degradation. In the case of the $[M(H_2O)PW_{11}O_{39}]^{5-}$-APS-$TiO_2$, it did not exhibit any

visible-light photocatalytic activity to dye degradation although its UV-light photocatalytic activity was very high to dye degradation. The reason for this may be due to lower BET specific surface area of the $[M(H_2O)PW_{11}O_{39}]^{5-}$-APS-$TiO_2$ than that of the $H_3PW_{12}O_{40}$/TiO_2 (Table 1). Certainly, the composition of the POM (substituted or saturated Keggin unit) also had an effect on the photocatalytic activity of the composites.

4.5. Evaluation

From the standpoint of separation and recovery of the catalyst in a large-scale wastewater treatment, the POM-containing film catalysts are more predominant than that of the powder catalysts since no separation process is needed for the films. As for the stability of the polyanions on the supporters, selecting lacunary or substituted POM as the inorganic precursors is better than the saturated POM. Therefore, the strong chemical interactions between the lacunary or substituted POM unit and the matrix (formation of the covalent or coordination bond) would avoid effectively the leakage of the active component from the matrix. However, the photocalytic activity of the saturated POM is somewhat higher than that of the lacunary or substituted one.

5. Future

Design and preparation of novel POM-containing composite photocatalysts with new composition, structure and fascinating physico-chemical properties as well as unusual morphology is still interesting targets for the future, while development of new soft chemical preparation techniques is needed. From the viewpoint of practical applications, preparation of the visible-light-driven POM-containing photocatalysts and control their composition and structure as well as improvement the stability of polyanions on the supports are important subjects. In addition, understanding and reasonably explaining the mechanism of the reaction performed under visible-light irradiation the solid POM are another urgent topics.

Acknowledgments

The Natural Science Found Council of China is acknowledged for financial support (NSFC 20331010, 20271007, and 90406002). This work were also supported by the Program of New Century Excellent Talents in University (NCET-04-0311) and Specialized Research Fund for the Doctoral Program of Higher Education of China (20030007014).

References

[1] J.-M. Herrmann, Catal. Today 53 (1999) 115.
[2] M. Vautier, C. Guillard, J.-M. Herrmann, J. Catal. 201 (2001) 46.
[3] C. Hu, Y. Wang, H. Tang, Appl. Catal. B 35 (2001) 95.
[4] M.R. Hoffmann, S.T. Mrtin, W.Y. Choi, D.W. Bahnemann, Chem. Rev. 95 (1995) 69.
[5] K.E. O'shea, S. Beightal, I. Garcia, M. Aguilar, D.V. Kalen, W.J. Cooper, J. Photochem. Photobiol. A 107 (1996) 221.
[6] T. Okuhara, Appl. Catal. A 256 (2003) 213.
[7] M.T. Pope, A. Müller, Angew. Chem. Int. Ed. Engl. 30 (1991) 34.
[8] N. Mizuno, M. Misono, Chem. Rev. 98 (1998) 199.
[9] I.V. Kozhevnikov, Chem. Rev. 98 (1998) 171.
[10] D.E. Katsoulis, Chem. Rev. 98 (1998) 359.
[11] E.F. Kozhevnikova, I.V. Kozhevnikov, J. Catal. 228 (2004) 174.
[12] M. Misono, Chem. Commun. (2001) 1141.
[13] C. Hu, M. Hashimoto, T. Okuhara, M. Misono, J. Catal. 143 (1993) 437.
[14] D. Sattair, C.L. Hill, J. Chem. Soc., Chem. Commun. (1990) 634.
[15] D. Sattari, C.L. Hill, J. Am. Chem. Soc. 115 (1993) 4649.
[16] C.L. Hill, Chem. Rev. 98 (1998) 1.
[17] A. Hiskia, A. Mylonas, E. Papaconstantinou, Chem. Soc. Rev. 30 (2001) 62.
[18] E. Papaconstantinou, Chem. Soc. Rev. 18 (1989) 1.
[19] M.A. Fox, R. Cardona, E. Gaillard, J. Am. Chem. Soc. 109 (1987) 6347.
[20] C.L. Hill, D.A. Bouchard, J. Am. Chem. Soc. 107 (1985) 5148.
[21] R.F. Renneke, C.L. Hill, J. Am. Chem. Soc. 108 (1986) 3528.
[22] T. Yamase, T. Usami, J. Chem. Soc., Dalton Trans. (1988) 183.
[23] A. Mylonas, E. Papaconstantinou, J. Photochem. Photobiol. A 94 (1996) 77.
[24] A. Mylonas, E. Papaconstantinou, J. Mol. Catal. 92 (1994) 261.
[25] C. Hu, B. Yue, T. Yamase, Appl. Catal. A 194–195 (2000) 99.
[26] A. Molinari, R. Amadelli, L. Andreotti, A. Maldotti, J. Chem. Soc., Dalton Trans. (1999) 1203.
[27] I.V. Kozhevnikov, A. Sinnema, R.J.J. Jansen, H.V. Bekkum, Catal. Lett. 27 (1994) 187.
[28] M. Verhoef, P.J. Kooyman, J.A. Peters, H.V. Bekkum, Micropor. Mesopor. Mater. 27 (1999) 365.
[29] R.R. Ozer, J.L. Ferry, Environ. Sci. Technol. 35 (2001) 3242.
[30] M. Bonchio, M. Carraro, G. Scorrano, E. Fontananova, E. Drioli, Adv. Synth. Catal. 345 (2003) 1119.
[31] R.R. Ozer, J.L. Ferry, J. Phys. Chem. B 106 (2002) 4336.
[32] B. Yue, Y. Zhou, J. Xu, Z. Wu, X. Zhang, Y. Zou, S. Jin, Environ. Sci. Technol. 36 (2002) 1325.
[33] T. Okuhara, T. Nishimura, H. Watanabe, M. Misono, Stud. Surf. Sci. Catal. 90 (1994) 419.
[34] T. Okuhara, T. Nishimura, M. Misono, Chem. Lett. (1995) 155.
[35] Y. Izumi, M. Ono, M. Ogawa, K. Urabe, Chem. Lett. (1993) 825.
[36] T. Okuhara, Chem. Rev. 102 (2002) 3641.
[37] D.A. Friesen, D.B. Gibson, C.H. Langford, Chem. Commun. (1998) 543.
[38] Y. Guo, C. Hu, J. Cluster Sci. 14 (2003) 505.
[39] Y. Guo, C. Hu, X. Wang, E. Wang, Y. Zhou, S. Feng, Chem. Mater. 13 (2001) 4058.
[40] Y. Guo, D. Li, C. Hu, Y. Wang, E. Wang, Appl. Catal. B 3–4 (2001) 337.
[41] Y. Guo, C. Hu, C. Jiang, Y. Yang, S. Jiang, X. Li, E. Wang, J. Catal. 217 (2003) 141.
[42] Y. Guo, Y. Yang, C. Hu, C. Guo, E. Wang, Y. Zhou, S. Feng, J. Mater. Chem. 12 (2002) 3046.
[43] Y. Yang, Y. Guo, C. Hu, C. Jiang, E. Wang, J. Mater. Chem. 13 (2003) 1686.
[44] Y. Guo, C. Hu, S. Jiang, C. Guo, Y. Yang, E. Wang, Appl. Catal. B 36 (2002) 9.
[45] Y. Guo, Y. Wang, C. Hu, E. Wang, Chem. Mater. 12 (2000) 3501.
[46] Y. Guo, D. Li, C. Hu, Y. Wang, E. Wang, Y. Zhou, S. Feng, Micropor. Mesopor. Mater. 56 (2002) 153.
[47] Y. Guo, D. Li, C. Hu, Y. Wang, E. Wang, Inter. J. Inorg. Mater. 3 (2001) 347.
[48] Y. Yang, Q. Wu, Y. Guo, C. Hu, E. Wang, J. Mol. Catal. A 225 (2005) 203.
[49] L. Li, Q. Wu, Y. Guo, C. Hu, Micropor. Mesopor. Mater. 87 (2005) 1.
[50] A.P. Wight, M.E. Davis, Chem. Rev. 102 (2002) 3589.
[51] Y. Yang, Y. Guo, C. Hu, Y. Wang, E. Wang, Appl. Catal. A 273 (2004) 201.
[52] L. Li, C. Liu, C. Jiang, Y. Guo, C. Hu, Mater. Res. Bull. 41 (2006) 319.
[53] R. Neumann, C.J. Abu-Gnim, Chem. Soc., Chem. Commun. (1989) 1324.
[54] A.M. Khenkin, C.L. Hill, J. Am. Chem. Soc. 115 (1993) 8178.
[55] D. Li, T. Yuranova, P. Albersb, J. Kiwi, Water Res. 38 (2004) 3541.
[56] L. Cheng, L. Niu, J. Gong, S. Dong, Chem. Mater. 11 (1999) 1465.
[57] D.G. Kurth, D. Volkmer, M. Ruttorf, B. Richter, A. Müller, Chem. Mater. 12 (2000) 2829.
[58] F. Caruso, D.G. Kurth, D. Volkmer, M.J. Koop, A. Müller, Langmuir 14 (1998) 3462.

[59] G. Decher, Science 277 (1997) 1232.
[60] A. Wu, D. Talham, Langmuir 16 (2000) 7449.
[61] Z. Tang, S. Liu, S. Dong, E. Wang, Langmuir 16 (2000) 5806.
[62] D. Dumitriu, A.R. Bally, C. Ballif, P. Hones, P.E. Schmid, R. Sanjinés, F. Lévy, V.I. Pârvulescu, Appl. Catal. B 25 (2000) 83.
[63] Y. Yano, K. lijima, Y. Daitoh, T. Terashima, Y. Bando, Y. Watanabe, H. Kasatani, H. Terauchi, J. Appl. Phys. 76 (1994) 7833.
[64] D. Li, Y. Guo, C. Hu, L. Mao, Appl. Catal. A 235 (2002) 11.
[65] D. Li, Y. Guo, C. Hu, J. Mol. Catal. A 207 (2004) 181.
[66] Y. Yang, Y. Guo, C. Hu, C. Guo, E. Wang, Appl. Catal. A 252 (2003) 305.
[67] B.T. Holland, C.F. Blanford, A. Stein, Science 281 (1998) 538.
[68] O.D. Velev, T.A. Jede, R.F. Lobo, A.M. Lenhoff, Chem. Mater. 10 (1998) 3579.
[69] Y. Xia, B. Gates, Y. Yin, Y. Lu, Adv. Mater. 12 (2000) 693.
[70] O.D. Velev, E.W. Kaler, Adv. Mater. 12 (2000) 531.
[71] J.E.G.J. Wijnhoven, S.J.M. Zevenhuizen, M.A. Hendriks, D. Vanmaekelbergh, J.J. Kelly, W.L. Vos, Adv. Mater. 12 (2000) 888.
[72] P.V. Braun, P. Wiltzius, Nature 402 (1999) 603.
[73] Q.B. Meng, Z.Z. Gu, O. Sato, A. Fujishima, Appl. Phys. Lett. 77 (2000) 4313.
[74] E. Wang, C. Hu, L. Xu, in: H. Liang (Ed.), Introduction of Polyoxometalates Chemistry, Chemical Industry Press, Beijing, China, 1997, pp. 19 and 40.
[75] Y. Yang, Y. Guo, C. Hu, Y. Wang, E. Wang, Appl. Catal. A 273 (2004) 201.
[76] K.N.P. Kumar, J. Kumar, K. Keizer, J. Am. Chem. Soc. 77 (1994) 1396.
[77] J. Yu, J.C. Yu, M.K.-P. Leung, W. Ho, B. Cheng, X. Zhao, J. Zhao, J. Catal. 217 (2003) 69.
[78] M. Fournier, H. Mourad, J. Mol. Catal. A 114 (1996) 53.
[79] T. Yamase, T. Kurozumi, J. Chem. Soc., Dalton Trans. (1983) 2205.
[80] M. Yoon, J.A. Chang, Y. Kim, J.R. Choi, K. Kim, S.J. Lee, J. Phys. Chem. B 105 (2001) 2539.
[81] J. Ryu, W. Choi, Environ. Sci. Technol. 38 (2004) 2928.
[82] H. Park, W. Choi, J. Phys. Chem. B 107 (2003) 3885.
[83] Y. Cao, W. Yang, W. Zhang, G. Liu, P. Yue, New. J. Chem. 28 (2004) 218.